Est. 1984

ORIENTAL JOURNAL OF CHEMISTRY
An International Open Access, Peer Reviewed Research Journal

www.orientjchem.org

ISSN: 0970-020 X
CODEN: OJCHEG
2019, Vol. 35, No.(3):
Pg. 1054-1061

Rhodamine-triazole Functionalized Fe_3O_4@SiO_2 Nanoparticles as Fluorescent Sensors for Heavy Metal Ions

KANOKORN WECHAKORN[1]*, PAIRSUNAN CHANPANICH[2], PIMFA KAMKALONG[2] and SURANAN ANANTACHISILP[2]

[1]Department of Chemistry, Faculty of Science and Technology, Rajamangala University of Technology Thanyaburi, Pathum Thani 12110, Thailand.
[2]Kamnoetvidya Science Academy, Rayong 21210, Thailand.
*Corresponding author E-mail: kanokorn_w@rmutt.ac.th

http://dx.doi.org/10.13005/ojc/350318

(Received: May 30, 2019; Accepted: June 06, 2019)

ABSTRACT

Rhodamine-triazole sensor functionalized Fe_3O_4@SiO_2 nanoparticles were developed for the detection of heavy metal ions, namely Cu^{2+}, Ni^{2+}, Hg^{2+}, Co^{2+}, Fe^{3+}, and Pb^{2+}. Rhodamine conjugated with a triazole moiety (RBT) was utilized as the metal ion binding site. The RBT-Fe_3O_4@SiO_2 nanoparticles were fully characterized by XRD, FTIR, TGA, SEM and TEM techniques. Additionally, RBT-functionalized Fe_3O_4@SiO_2 nanoparticles can be separated from aqueous phase by application of an external magnet, leading to clear naked-eye observation of the color changes and fluorescence enhancement. From UV-Vis absorption spectra, aqueous solutions of RBT-Fe_3O_4@SiO_2 in the presence of heavy metal ions show an absorption peak at 554 nm. Fluorescence titration experiments reveal that the intensity of the fluorescence emission band at 574 nm is linearly dependent on Cu^{2+} concentration over a 100–800 µM range. Furthermore, complexation of Cu^{2+} by RBT-Fe_3O_4@SiO_2 nanoparticles can induce ring-opening of the rhodamine spirolactam ring followed by hydrolysis, confirmed by mass spectrometry.

Keywords: Fluorescent sensor, Magnetic nanoparticles, Heavy metal ions, Triazole, Rhodamine.

INTRODUCTION

Contamination of water sources by heavy metal ions (e.g. Co^{2+}, Cu^{2+}, Fe^{3+}, Hg^{2+}, Ni^{2+} and Pb^{2+}) is a major environmental concern. In addition, their toxicity and accumulation in living organisms can have profound impacts on the overall ecology of environmental systems. Accordingly, great effort is being extended into devising ways of removing such pollutants and the development of new analytical tools for their detection. Although conventional analytical techniques such as atomic absorption spectrometry (AAS)[1], flame atomic absorption spectroscopy (FAAS)[2], inductively coupled plasma mass spectrometry (ICP-MS)[3] and voltammetry[4] are typically used in metal ion detection, they have drawbacks in requiring expensive and sophisticated hardware, long analysis time, and a high level of technical expertise. Fluorescence spectroscopy, on the other hand, is an emerging technique for metal

ion detection in environmental science due to its high selectivity, rapid response allowing real-time detection for potential field use and low cost[5].

Over the last decade, magnetic nanoparticles have been extensively studied since they have large surface area to volume ratios and are readily separated from liquid phase by application of an external field. Conjugation of organic groups on the nanoparticle surface allows these systems to be utilized in analytical applications such as metal ion detection. For example, amino-functionalized $Fe_3O_4@SiO_2$ magnetic nanomaterials were developed as sorbents for the toxic metal ions including Cu^{2+}, Pb^{2+}, and Cd^{2+} ions[6-9]. In addition, thiol-functionalized $Fe_3O_4@SiO_2$ nanoparticles were synthesized for Pb^{2+} and Hg^{2+} sequestration from water samples[10-13]. Appending fluorescent groups (dansyl, naphthalimide, Nile red, or BODIPY) to the nanoparticle surface allows the potential of fluorescence as a detection method to be built into the nanoparticle system. As an example, Ma's group developed reusable dansyl-functionalized $Fe_3O_4@SiO_2$ nanoparticles for Hg^{2+} detection, and subsequent removal from water samples[14]. In this case, the fluorescence intensity of nanoparticles was quenched in the presence of Hg^{2+}, with the limit of detection being 10 μM in HEPES buffer containing 50% (v/v) CH_3CN/H_2O. In 2013, "Turn-off" naphthalimide functionalized $Fe_3O_4@SiO_2$ nanoparticles were observed to aggregate in the presence of Hg^{2+}, forming imide-Hg-imide complexes in aqueous solution[15]. In another development, Zhu's group designed thioether-crown conjugated naphthalimide modified $Fe_3O_4@SiO_2$ nanoparticles via click chemistry for Hg^{2+} sensing[16]. Recently, magnetic nanoparticles appended with 4-acetamidobenzaldehyde functionalities were able to detect Hg^{2+} at the nanomolar level[17]. Meanwhile, dipicolylamine-naphthalimide conjugated magnetic nanoparticles exhibited fluorescence emission allowing feasible Zn^{2+} detection in environmental water samples[18]. In the case of Co^{2+} ion, chelation by Nile red-functionalized $Fe_3O_4@SiO_2$ nanoparticles leads to fluorescence emission through the inhibition of photoinduced electron transfer (PET)[14].

Rhodamine derivatives have been widely reported as fluorescent entities due to their long absorption and emission wavelengths, large molar extinction coefficients, high fluorescence quantum yields and appreciable photostability[19]. In these systems, rhodamine having the closed-form of the spirolactam ring is colorless and shows no fluorescence emission, while the solutions of the open-form of rhodamine exhibit a pink color and fluorescence emission. As a consequence, rhodamine has been appended to the surface of magnetic nanoparticles to form sensors for Fe^{3+} and Hg^{2+}. In 2010, rhodamine 6G-ethylenediamine was conjugated to the surface of $Fe_3O_4@SiO_2$ nanoparticles via a polyethylene linker, which exhibited fluorescence emissions in the presence of Fe^{3+} ion[20]. Substituting the polyethylene linker in the previous system by an isocyanate linker resulted in the selectivity of the sensor with the binding of Hg^{2+}, Cr^{3+} and Fe^{3+} ions[21,22]. In the context of Hg^{2+} removal, rhodamine hydrazide was grafted onto the magnetic nanoparticle surface via 3-glycidyloxy moiety[23], or chloroacetyl aminopropane linkers[24]. From the previous literatures, rhodamine-based fluorescent sensor immobilized on the magnetic nanoparticles have not been widely developed for heavy metal ion detection.

This work reports the synthesis of a rhodamine-triazole sensor appended $Fe_3O_4@SiO_2$ nanoparticles for the detection of heavy metal ions (Cu^{2+}, Ni^{2+}, Hg^{2+}, Co^{2+}, Fe^{3+} and Pb^{2+}). The sensor-functionalized nanoparticles could be easily removed from the solution by applying an external magnetic field. Additionally, the 1,2,3-triazole moiety plays several important roles, being both the metal chelator and the linker between the fluorescence reporter and the metal ion binding site[25]. The selectivity and sensitivity of the sensor system as well as a rationale for the sensing mechanism, are also reported herein.

MATERIALS AND METHODS

Materials and Instruments

All chemicals and reagents of standard analytical grade were purchased from commercial suppliers and used without further purification. All solvents for column chromatography were distilled before use. The stock solutions (10 mM) of the metal ions including Co^{2+}, Cu^{2+}, Fe^{2+}, Fe^{3+}, Hg^{2+}, Ni^{2+} and Pb^{2+} were prepared in deionized water from their acetate salt.

^1H and ^{13}C NMR spectra were recorded on an Advance Bruker-600AV spectrometer in

$CDCl_3$ with tetramethylsilane (TMS) as an internal reference. Fourier transform infrared (FT-IR) spectra were collected on a Perkin Elmer Spectrum two spectrometer using KBr pellets in the 4000–370 cm^{-1} region. High resolution mass spectra (HRMS) were obtained on a Bruker MicrOTOF mass spectrometer. Scanning electron microscope (SEM) images were obtained on a Jeol JAM-7610F with normal mode and EDS mode. Transmission electron microscopy (TEM) images were performed on a Jeol JEM-2100Plus electron microscope. X-ray diffraction (XRD) studies were performed on a Bruker d8 Venture powder diffractometer (2theta 20 to 80^O) with Cu Kα radiation. Thermogravimetric analysis (TGA) was utilized on a Linseis STA PT1600 instrument. UV-Vis absorption spectra were measured on a Hitachi U-2900/2910 UV-Visible spectrophotometer. Fluorescence spectra were performed on an Edinburgh fluorescence lifetime spectrometer.

Synthesis of silica-coated magnetic nanoparticles (Fe_3O_4@SiO_2)

The magnetic nanoparticles were synthesized according to a previously reported procedure[26]. Briefly, a solution of $Fe(acac)_3$ (5.65 g, 0.016 mol), benzyl ether (80 mL) and oleylamine (80 mL) was heated to 110 ^{O}C and allowed to reflux for 1 h with vigorous stirring. The temperature was raised to 210 ^{O}C and then refluxed for 2 h under an argon atmosphere. After cooling to room temperature, the reaction mixture was centrifuged at 10,000 rpm for 20 min, affording the magnetic nanoparticles (Fe_3O_4) as a black solid. The magnetic nanoparticles were then dispersed in a mixture of 1-propanol (180 mL), conc. NH_4OH (25 mL) and deionized water (18 mL) in a 500 mL round-bottom flask by ultra-sonication for 30 min under an argon atmosphere. Following this, tetraethylorthosilicate (TEOS) (6 mL, 0.027 mol) was added dropwise for 30 min with vigorous stirring. After stirring at room temperature for 6 h, the silica-coated magnetic nanoparticles (Fe_3O_4@SiO_2) were separated from the solution using an external magnet and then washed twice successively with 1-propanol and deionized water, respectively. The Fe_3O_4@SiO_2 nanoparticles (brown solid) were then dried under vacuum at 60 ^{O}C for 6 h, prior to use.

Synthesis of 3-azidopropyl triethoxysilane

3-Chloropropyl triethoxysilane (5 mL, 0.021 mol) and sodium azide (NaN_3) (2.70 g, 0.042 mol, 2 equiv.) were dissolved in DMF (40 mL), and the mixture was heated at 90 ^{O}C for 6 h. After that the mixture was filtered and the filtrate was evaporated under reduced pressure to provide the product as a colorless liquid in 90% yield. ^{1}H NMR (600 MHz, $CDCl_3$) δ (ppm): 3.80 (d, J = 6 Hz, 6H), 3.24 (d, J = 6 Hz, 2H), 1.70 (d, J = 6 Hz, 2H), 1.21 (t, J = 6 Hz, 9H), 0.66 (t, J = 6 Hz, 2H); ^{13}C NMR (150 MHz, $CDCl_3$) δ (ppm): 58.5, 53.9, 22.8, 18.3, 7.7.

Synthesis of Rhodamine-*N*-propargyl alkyne

Rhodamine-*N*-propargyl alkyne was prepared according to a previously reported procedure[27]. The crude product was purified by silica column chromatography with 1% (v/v) CH_3OH/CH_2Cl_2 system as a mobile phase to obtain a light brown solid in 75% yield. ^{1}H NMR (600 MHz, $CDCl_3$) δ (ppm): 7. 91. (d, J = 6 Hz, 1H), 7.45 (s, 2H), 7.1 (d, J = 6 Hz, 1H), 6.41–6.46 (m, 4H), 6.27 (d, J = 6 Hz, 4H), 4.57 (s, 1H), 3.32 (t, J = 6 Hz, 10H), 2.10 (s, 1H), 1.16 (t, J = 6 Hz,12H); ^{13}C NMR (150 MHz, $CDCl_3$) δ (ppm): 166.64, 153.70, 151.78, 149.52, 148.84, 132.75, 129.83, 128.54, 128.51, 128.10, 123.98, 122.89, 122.86, 109.74, 107.86, 105.65, 100.07, 98.46, 80.10, 72.42, 65.43, 45.53, 44.44, 44.34, 40.42, 12.63.

Synthesis of chemosensor-functionalized magnetic nanoparticles (RBT-Fe_3O_4@SiO_2)

The Fe_3O_4@SiO_2 nanoparticles (1.5 g) were suspended in toluene (80 mL) under an argon atmosphere, and then sonicated for 30 min. 3-Azidopropyl triethoxysilane (1.5 g, 6.1 mmol) was slowly added dropwise into the mixture for 15 min and the mixture was then heated at reflux for 12 h. The Fe_3O_4@SiO_2-N_3 nanoparticles were then separated by applying an external magnet and then washed three times successively with toluene, 1-propanol and deionized water (30 mL), respectively. Subsequently, the Fe_3O_4@SiO_2-N_3 nanoparticles were dispersed in acetonitrile (50 mL) with the sonication for 30 min while maintaining an argon atmosphere. In a separate flask, a solution of rhodamine-*N*-propargyl alkyne derivative (0.5 g, 1 mmol) and $CuBr(PPh_3)_3$ (50 mg, 0.05 mmol) in acetonitrile (50 mL) was prepared and after being stirred for 30 min then it was added into the Fe_3O_4@SiO_2-N_3 nanoparticle dispersion with vigorous stirring under an argon atmosphere. After 24 h, the RBT-Fe_3O_4@SiO_2 nanoparticles were separated using an external magnet and washed twice successively with acetonitrile, methanol and dichloromethane (15 mL), respectively.

RESULTS AND DISCUSSION

RBT-functionalized Fe_3O_4@SiO_2 nanoparticles were synthesized by the click chemistry protocol (copper(I)-catalyzed azide alkyne cycloaddition, CuAAC) which involved grafting rhodamine-*N*-propargyl alkyne moieties on the surface of Fe_3O_4@SiO_2 nanoparticles[27]. Rhodamine-*N*-propargyl alkyne was synthesized in good yield from the condensation of rhodamine B with hydrazine to obtain rhodamine hydrazide, followed by nucleophilic substitution with electrophilic propargyl bromide, as shown in Scheme 1. Magnetic nanoparticles (Fe_3O_4) were prepared from a thermal decomposition process and the surface of the Fe_3O_4 nanoparticles was coated with silica via a sol-gel process. Subsequent appending of azide groups to the silica surface, followed by application of the click chemistry protocol (CuAAC) with rhodamine-*N*-propargyl alkyne afforded RBT-Fe_3O_4@SiO_2 nanoparticles.

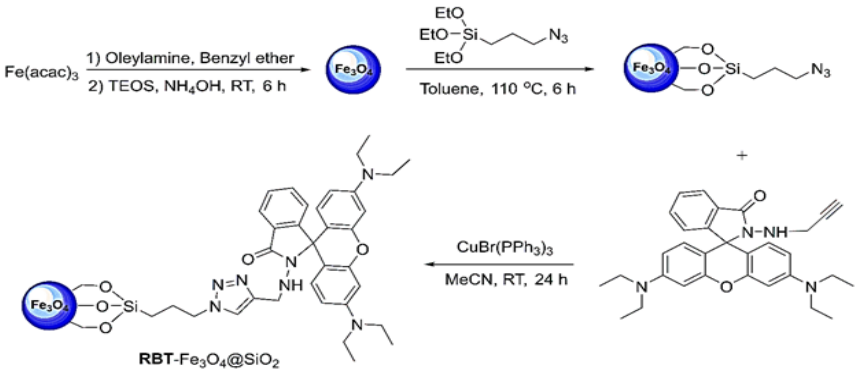

Scheme 1. Synthesis of RBT-functionalized Fe_3O_4@SiO_2 nanoparticles

The presence of RBT on the surface of the Fe_3O_4@SiO_2 nanoparticles was confirmed by FT-IR spectroscopy, as highlighted in Fig.1. Both Fe_3O_4@SiO_2 and RBT-Fe_3O_4@SiO_2 nanoparticles exhibit characteristic Fe–O stretching frequencies at 592 cm^{-1} and 586 cm^{-1}, respectively. Absorption peaks at 797 cm^{-1}, 963 cm^{-1} and 1104 cm^{-1} in RBT-Fe_3O_4@SiO_2 nanoparticles are assigned to Si–O stretching vibrations which are also observed in Fe_3O_4@SiO_2 nanoparticles (797 cm^{-1}, 956 cm^{-1} and 1101 cm^{-1}). Strong intensity bands at 468 cm^{-1} and 464 cm^{-1}, ascribed to Si–O–Si bending are presented in Fe_3O_4@SiO_2 and RBT-Fe_3O_4@SiO_2 nanoparticles, respectively. The absorption bands around 1634 cm^{-1} in Fe_3O_4@SiO_2 nanoparticles and 1628 cm^{-1} in RBT-Fe_3O_4@SiO_2 nanoparticles can be attributed to O–H bonds in silanol groups. Furthermore, the FT-IR spectrum of RBT-Fe_3O_4@SiO_2 nanoparticles shows absorption peaks at 635 cm^{-1}, 1397 cm^{-1}, 1490 cm^{-1} and 1573 cm^{-1} which can be assigned to C–H bending in aromatic groups, alkyl (C–H) bending, aromatic C=C stretching, and aromatic C=C bending, respectively, consistent with surface functionalization of nanoparticles with rhodamine-triazole entities. TGA analysis of RBT-Fe_3O_4@SiO_2 nanoparticles was further confirmed the presence of organic functional groups on the surface. From the TGA curves in Fig. 2, initial weight loss occurred below 200 °C consistent with removal of adsorbed water. Thermal decomposition of RBT-Fe_3O_4@SiO_2 occurs at 450–560 °C with a total weight loss of 10.2%, in contrast to < 1% for both Fe_3O_4@SiO_2 and azide-Fe_3O_4@SiO_2 nanoparticles.

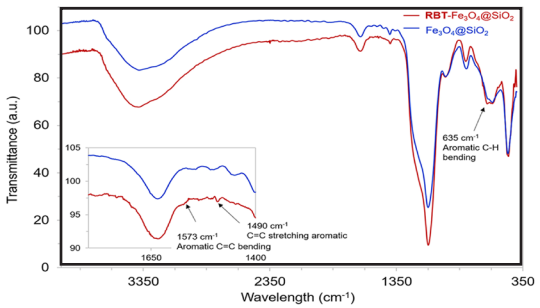

Fig. 1. FT-IR spectra of Fe_3O_4@SiO_2 (blue line) and RBT-Fe_3O_4@SiO_2 (red line)

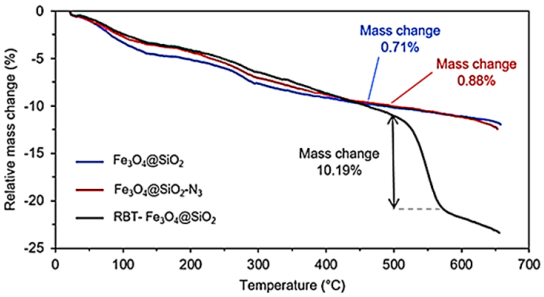

Fig. 2. TGA curves of (a) Fe_3O_4@SiO_2 (blue line), (b) Fe_3O_4@SiO_2-N_3 (red line) and (c) RBT-Fe_3O_4@SiO_2 nanoparticles (black line)

The magnetic property of Fe_3O_4@SiO_2 nanoparticles was proved by XRD analysis. XRD pattern in Fig. 3 shows the characteristic diffraction peaks of magnetite Fe_3O_4 nanoparticles at (220), (311), (400), (511), (440) and (533), corresponding to previous reports[28,29]. Silica shows a broad peak around 20–28° suggesting that Fe_3O_4 nanoparticles were coated with silica.

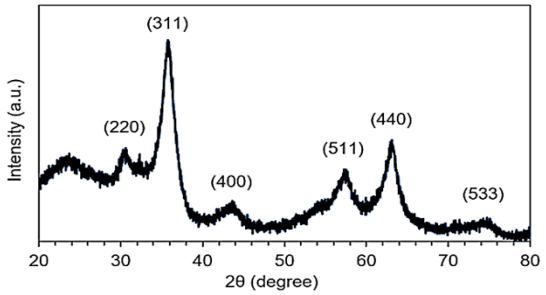

Fig. 3. XRD pattern of Fe_3O_4@SiO_2 nanoparticles

The morphologies of the RBT-functionalized Fe_3O_4@SiO_2 nanoparticles were observed using SEM imaging (Fig. 4). Magnetic Fe_3O_4 nanoparticles are spherical with the diameter approximately at 67 nm (Fig. 4a). After the modification, silica-coated Fe_3O_4 nanoparticles (Fig. 4b) and RBT-functionalized Fe_3O_4@SiO_2 nanoparticles (Fig. 4c) also remain spherical, but they have larger sizes as expected from the addition of surface coatings, respectively. The size of RBT-Fe_3O_4@SiO_2 nanoparticles was elucidated by TEM image. Fig. 4d shows that the average diameter of the RBT-Fe_3O_4@SiO_2 nanoparticles was about 155 nm. EDX analysis and elemental mapping of the Fe_3O_4@SiO_2 nanoparticles provide a further insight into their composition with the elemental distribution of iron (Fe) and silica (Si), as highlighted in Fig. 5b. The atomic percentages of carbon (C, 62.73%), oxygen (O, 30.06%), silica (Si, 4.33%), and iron (Fe, 2.87%) for RBT-Fe_3O_4@SiO_2 nanoparticles are indicative of the existence of organic and silica surface layers, as shown in Fig. 5c.

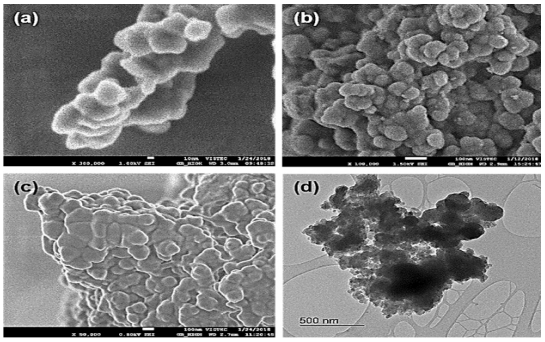

Fig. 4. SEM images of (a) Fe_3O_4, (b) Fe_3O_4@SiO_2, and (c) RBT-Fe_3O_4@SiO_2 nanoparticles, and (d) TEM image of RBT-Fe_3O_4@SiO_2 nanoparticles

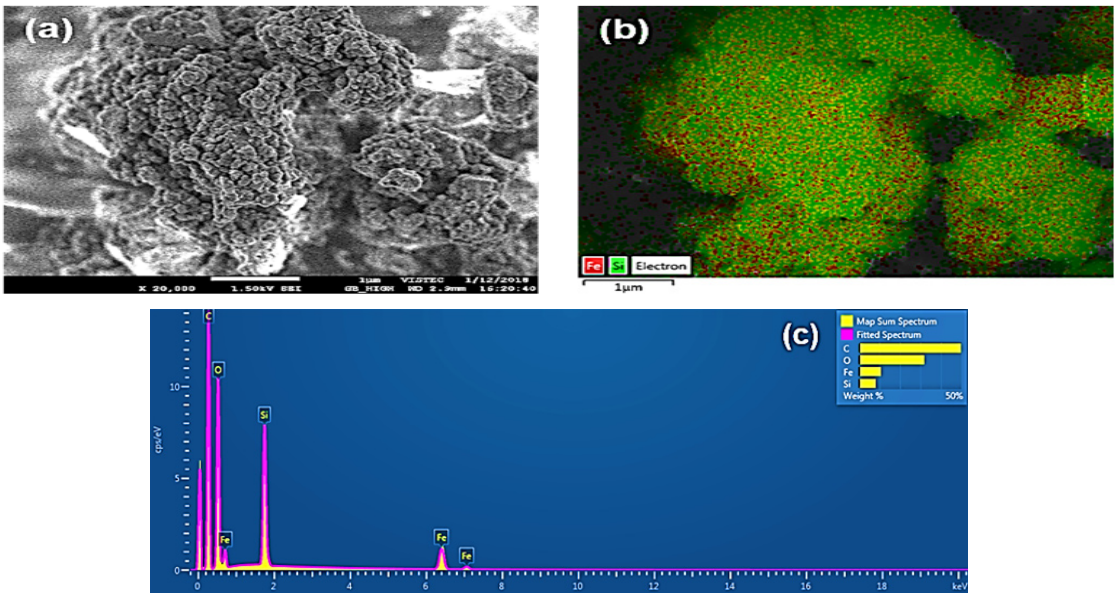

Fig. 5. SEM images of Fe_3O_4@SiO_2 in (a) normal mode, (b) EDS mode showing Fe (red), Si (green), and (c) the EDS mapping profile of Fe_3O_4@SiO_2 depicting elemental ratios

The selectivity of RBT-Fe_3O_4@SiO_2 nanoparticles towards sensing of heavy metal ions (Cu^{2+}, Ni^{2+}, Hg^{2+}, Co^{2+}, Fe^{2+}, Fe^{3+} and Pb^{2+}) in MeOH/H_2O (9:1, v/v) was investigated by UV absorption

and fluorescence measurements. While initially exhibiting colorless, the RBT-Fe_3O_4@SiO_2 solutions exhibit visible color changes on the addition of metal ions, becoming pink in the presence of Cu^{2+}, Co^{2+}, Ni^{2+} ions, and pink-orange when challenged with Hg^{2+}, Pb^{2+} and Fe^{3+} ions (Fig. 7b). However, no change results from the presence of Fe^{2+} ion. From Fig. 7a, the RBT-Fe_3O_4@SiO_2 solutions exhibit an absorption maximum at 554 nm when exposed to all of the above metal ions, with Fe^{3+} ion resulting in the highest absorption intensities. Fluorescence spectra in Fig. 8a indicate that the RBT-Fe_3O_4@SiO_2 (control) solution is only weakly fluorescent on excitation at 530 nm. Nevertheless, the addition of metal ions with the exception of Fe^{2+} results in significant fluorescence enhancements with maximum emission wavelengths at 572 nm on addition of Co^{2+}, 574 nm for Cu^{2+} and Hg^{2+}, 576 nm for Ni^{2+}, 578 nm for Fe^{3+}, and 580 nm for Pb^{2+} ions. Furthermore, fluorescence enhancement of the RBT-Fe_3O_4@SiO_2 solution displayed 1.5-fold upon the addition of Cu^{2+} in MeOH/H_2O (9:1, v/v) by excitation at 530 nm, as shown in Fig. 8b. In case of Fe^{3+} ion, fluorescence emission revealed 0.8-fold compared to the absence of metal ions because of fluorescence quenching effect of Fe^{3+} ion. From these results, the RBT-Fe_3O_4@SiO_2 nanoparticles can act as a "naked-eye" colorimetric and fluorescent sensor for certain heavy metal ions (Cu^{2+}, Hg^{2+}, Co^{2+}, Fe^{3+} and Pb^{2+}).

Due to the fluorescence enhancement being greatest in the case of Cu^{2+}, the fluorescence response of the RBT-Fe_3O_4@SiO_2 nanoparticles to this metal ion was investigated in more detail using titration experiments (Fig. 9). From the fluorescence spectra in Fig. 9a, increasing the Cu^{2+} concentration results in fluorescence enhancements with the maximum intensity being reached at 800 μM. Excitation at 530 nm results in a linear relationship (Fig. 8b) ($y = 82.986X + 8677.2$, $R^2 = 0.9909$) at 574 nm between fluorescence intensity and Cu^{2+} concentration (range 100–800 μM). The detection limit was determined to be 9.8 μM based on $3\sigma/S$, where σ is the standard deviation of the fluorescence intensity of the RBT-Fe_3O_4@SiO_2 solution and S is the slope of the calibration curve. Moreover, naked eye color changes in the RBT-Fe_3O_4@SiO_2 solution were observable for Cu^{2+} ion concentrations > 50 μM, as shown in Fig. 9c.

The binding mechanism of Cu^{2+} to RBT-Fe_3O_4@SiO_2 nanoparticles in MeOH was further investigated by ESI-MS analysis, with the results shown in Fig. 10. As indicated above, the addition of these ions results in both color changes and fluorescence emission, resulting from the metal ions promoted ring-opening of the spirolactam ring in rhodamine[19]. The mass spectrum of the RBT-Fe_3O_4@SiO_2 solution in the presence of Cu^{2+} (in MeOH) displayed a new molecular ion peak at m/z of 457.2615, which is suggestive of formation of a rhodamine methyl ester (calcd for $C_{29}H_{33}N_2O_3$, 457. 2486). This outcome is consistent with rhodamine ring-opening followed by hydrolysis as postulated previously[27].

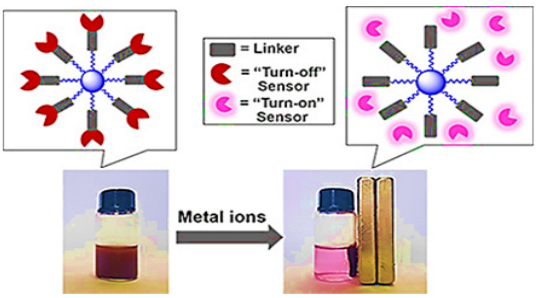

Fig. 6. Separation method of the RBT-Fe_3O_4@SiO_2 nanoparticles in the aqueous phase using an external magnet

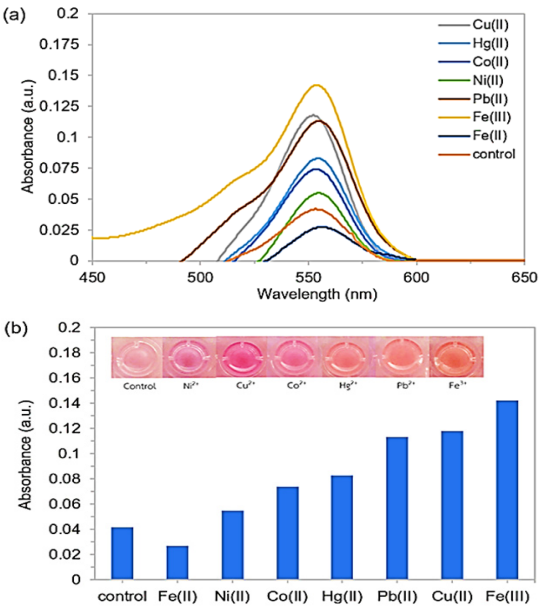

Fig. 7. (a) UV-absorption spectra of the RBT-Fe_3O_4@SiO_2 (20 mg) solutions in MeOH/H_2O (9:1, v/v) in the presence of various metal ions (1 mM), and (b) a bar graph showing the relative absorbance (554 nm) of the RBT-Fe_3O_4@SiO_2 (20 mg) solutions in the presence of these metal ions (1 mM), in MeOH/H_2O (9:1, v/v); Inset: Color changes of the RBT-Fe_3O_4@SiO_2 (20 mg) solutions on the addition of metal ions (1 mM), in MeOH/H_2O (9:1, v/v)

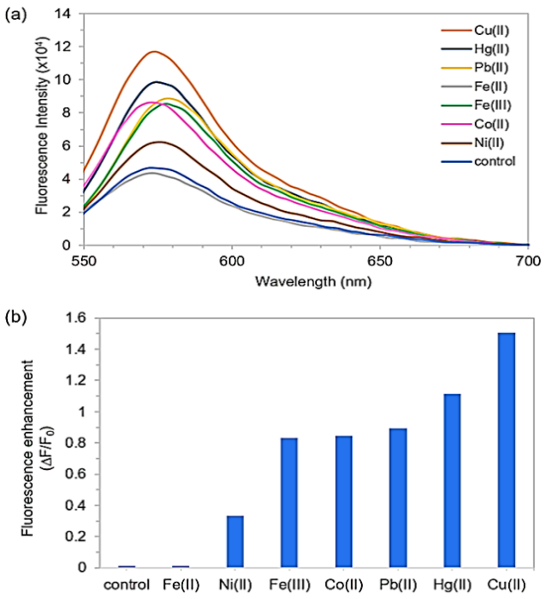

Fig. 8. (a) Fluorescence spectra obtained by excitation of the RBT-Fe_3O_4@SiO_2 (20 mg) solutions in MeOH/H_2O (9:1, v/v) at 530 nm in the presence of metal ions (1 mM), and (b) a bar graph depicting the relative fluorescence enhancement (574 nm) ($\Delta F/F_0$) of the RBT-Fe_3O_4@SiO_2 (20 mg) solutions on the addition of metal ions (1 mM) in MeOH/H_2O (9:1, v/v)

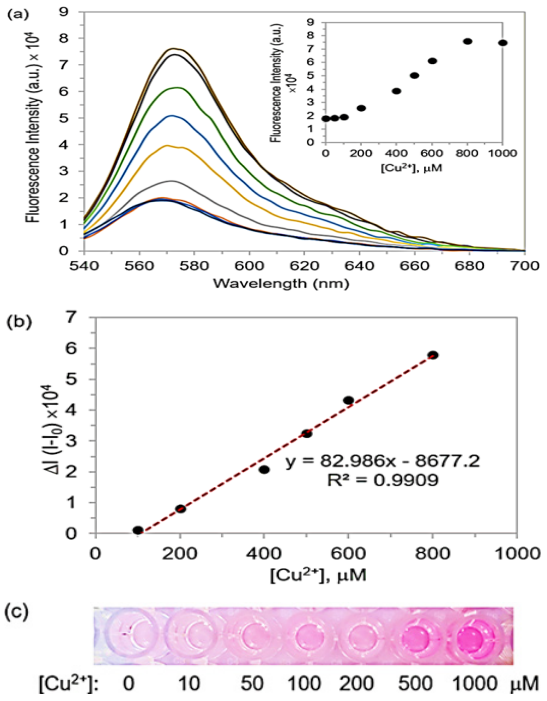

Fig. 9. (a) Fluorescence spectra obtained by excitation of the RBT-Fe_3O_4@SiO_2 (20 mg) solutions at 530 nm in MeOH/H_2O (9:1, v/v) with the addition of Cu^{2+} (10–1,000 μM), (b) calibration curve and (c) color changes of the RBT-Fe_3O_4@SiO_2 (20 mg) solutions in MeOH/H_2O (9:1, v/v) on the addition of Cu^{2+} (10–1,000 μM)

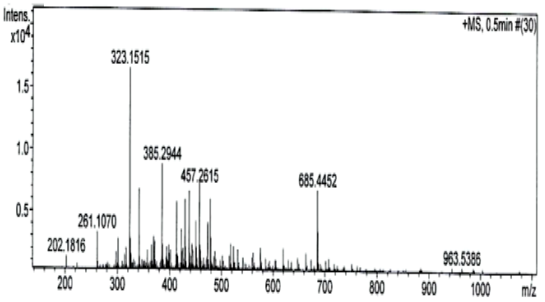

Fig. 10. Mass spectrum of the RBT-Fe_3O_4@SiO_2 (20 mg) solution upon the addition of Cu^{2+} in MeOH

CONCLUSION

We have successfully synthesized rhodamine-triazole functionalized Fe_3O_4@SiO_2 nanoparticles, based on the click chemistry approach. Upon the addition of heavy metal ions (Cu^{2+}, Co^{2+}, Ni^{2+}, Hg^{2+}, Fe^{3+}, and Pb^{2+}), the solutions of these nanoparticles exhibited distinct naked eye color changes (maximum absorption wavelength at 554 nm), and intense fluorescence emissions at 572–580 nm. As Cu^{2+} ion displayed optimum binding behavior, the limit of detection was found to be 9.8 μM with fluorescence responses showing a linear correlation with Cu^{2+} concentration in the range of 100 to 800 μM.

ACKNOWLEDGMENT

This work was financially supported by the Institute of Research and Development, Rajamangala University of Technology Thanyaburi (Project No. NRF62D0602). We wish to thank Assoc. Prof. Dr. Palangpon Kongsaeree (Department of Chemistry, Mahidol University) for experimental supports and Associate. Prof. Dr. Christopher Smith (Kamnoetvidya Science Academy) for his suggestions. We would also like to thank the Kamnoetvidya Science Academy (KVIS) and Vidyasirimedhi Institute of Science and Technology (VISTEC) for use of equipment for characterization purposes.

Conflict of Interest

The authors declare that they no conflict of interest.

REFERENCES

1. Soylak, M.; Divrikli, U.; Saracoglu, S.; Elci, L. *Environ. Monit. Assess.*, **2007**, *127*, 169-176.
2. Giokas, D. L.; Tsogas, G. Z.; Vlessidis, A. G.; Karayannis, M. I. *Anal. Chem.*, **2004**, *76*, 1302-1309.
3. Dressler, V. L.; Pozebon, D.; Curtius, A. *J. Spectrochim. Acta* B., **1998**, *53*, 1527-1539.
4. Lu, Y.; Liang, X.; Niyungeko, C.; Zhou, J.; Xu, J.; Tian, G. *Talanta.,* **2018**, *178*, 324-338.
5. Formica, M.; Fusi, V.; Giorgi, L.; Micheloni, M. *Coord. Chem. Rev.*, **2012**, *256*, 170-192.
6. Zhang, J.; Zhai, S.; Li, S.; Xiao, Z.; Song, Y.; An, Q.; Tian, G. *Chem. Eng. J.*, **2013**, *215-216*, 461-471.
7. Bao, S.; Tang, L.; Li, K.; Ning, P.; Peng, J.; Guo, H.; Zhu, T.; Liu, Y. *J. Colloid Interface Sci.*, **2016**, *462*, 235-242.
8. Meng, C.; Zhikun, W.; Qiang, L.; Chunling, L.; Shuangqing, S.; Songqing, H. *J. Hazard Mater.*, **2018**, *341*, 198-206.
9. Wang, J.; Zheng, S.; Shao, Y.; Liu, J.; Xu, Z.; Zhu, D. *J. Colloid Interface Sci.*, **2010**, *349*, 293-299.
10. Zhang, S.; Zhang, Y.; Liu, J.; Xu, Q.; Xiao, H.; Wang, X.; Xu, H.; Zhou, *J. Chem. Eng. J.,* **2013**, *226*, 30-38.
11. Wang, Z.; Xu, J.; Hu, Y.; Zhao, H.; Zhou, J.; Liu, Y.; Lou, Z.; Xu, X. *J. Taiwan Inst. Chem. Eng.*, **2016**, *60*, 394-402.
12. Villa, S.; Riani, P.; Soggia, F.; Magi, E.; Canepa, F. *J. Nanoparticle Res.*, **2019**, *21*, 44.
13. Hakami, O.; Zhang, Y.; Banks, C. *J. Water Res.*, **2012**, *46*, 3913-3922.
14. Ma, T.; Lv, Y.; Liu, H.; Lv, Y.; Tian, Z. *J. Nanoparticle Res.*, **2013**, *15*, 1933.
15. Zhu, B.; Zhao, J.; Yu, H.; Yan, L.; Wei, Q.; Du, B. *Chem. Eng. J.*, **2013**, *219*, 411-418.
16. Tang, Y.; Liu, Y.; Qin, Y.; Xu, Y.; Qian, X.; Zhu, W. *J. Colloid Interface Sci.*, **2016**, *479*, 7-14.
17. Heidari, A.; Mir, N. *J. Fluores.*, **2017**, *27*, 659-667.
18. Kim, K. T.; Yoon, S. A.; Ahn, J.; Choi, Y.; Lee, M. H.; Jung, J. H.; Park, J. *Sensors Actuat. B- Chem.*, **2017**, *243*, 1034-1041.
19. Chen, X.; Pradhan, T.; Wang, F.; Kim, J. S.; Yoon, *J. Chem. Rev.*, **2012**, *112*, 1910-1956.
20. Wang, B.; Hai, J.; Liu, Z.; Wang, Q.; Yang, Z.; Sun, S. *Angew. Chem. Int. Ed.*, **2010**, *49*, 4576-4579.
21. Peng, X.; Wang, Y.; Tang, X.; Liu, W. *Dyes Pigm.*, **2011**, *91*, 26-32.
22. Xu, Y.; Zhou, Y.; Ma, W.; Wang, S.; Li, S. *J. Nanoparticle Res.*, **2013**, *15*, 1716.
23. Tan, J.; Wei, X.; Chen, J.; Sun, P.; Ouyang, Y.; Fan, J.; Liu R. *Spectrochim. Acta* A., **2014**, *133*, 403-410.
24. Sun, Z. B.; Guo, D.; Li, H. Z.; Zhang, L.; Yang, B.; Yan, S. Q. *Rsc Adv.*, **2015**, *5*, 11000-11008.
25. Lau, Y. H.; Rutledge, P. J.; Watkinson, M.; Todd, M. H. *Chem. Soc. Rev.*, **2011**, *40*, 2848-2866.
26. Xu, Z.; Shen, C.; Hou, Y.; Gao, H.; Sun, S. *Chem. Mater.*, **2009**, *21*, 1778-1780.
27. Wechakorn, K.; Prabpai, S.; Suksen, K.; Kanjanasirirat, P.; Pewkliang, Y.; Borwornpinyo, S.; Kongsaeree, P. *Luminescene.,* **2018**, *33*, 64-70.
28. Lei, W.; Liu, Y.; Si, X.; Xu, J.; Du, W.; Yang, J.; Zhou, T.; Lin, *J. Phys. Lett.*, A **2017**, *381*, 314-318.
29. Xu, J.; Yang, H.; Fu, W.; Du, K.; Sui, Y.; Chen, J.; Zeng, Y.; Li, M.; Zou, G. J. Magn. *Magn. Mater.*, **2007**, *309*, 307-311.